

# Detailed spectroscopic and photometric study of three detached eclipsing binaries

F. Kahraman Aliçavuş<sup>1,2\*</sup>, F. Aliçavuş<sup>2</sup>

<sup>1</sup>*Nicolaus Copernicus Astronomical Center, Bartycka 18, PL-00-716 Warsaw, Poland*

<sup>2</sup>*Canakkale Onsekiz Mart University, Faculty of Sciences and Arts, Physics Department, 17100, Canakkale, Turkey*

Accepted ... Received ...; in original form ...

## ABSTRACT

Detached eclipsing binaries are remarkable systems to provide accurate fundamental stellar parameters. The fundamental stellar parameters and the metallicity values of stellar systems are needed to deeply understand the stellar evolution and formation. In this study, we focus on the detailed spectroscopic and photometric studies of three detached eclipsing binary systems, V372 And, V2080 Cyg, and CF Lyn to obtain their accurate stellar, atmospheric parameters, and chemical compositions. An analysis of light and radial velocity curves was carried out to derive the orbital and stellar parameters. The disentangled spectra of component stars were obtained for the spectroscopic analysis. Final  $T_{\text{eff}}$ ,  $\log g$ ,  $\xi$ ,  $v \sin i$  parameters and the element abundances of component stars were derived by using the spectrum synthesis method. The fundamental stellar parameters were determined with a high certainty for V372 And, V2080 Cyg ( $\sim 1 - 2\%$ ) and with an accuracy for CF Lyn ( $\sim 2 - 6\%$ ). The evolutionary status of the systems was examined and their ages were obtained. It was found that the component stars of V2080 Cyg have similar iron abundance which is slightly lower than solar iron abundance. Additionally, we showed that the primary component of CF Lyn exhibits a non-spherical shape with its 80% Roche lobe filling factor. It could be estimated that CF Lyn will start its first Roche overflow in the next 0.02 Gyr.

**Key words:** stars: general – stars: abundances – binaries: eclipsing – stars: atmospheres – stars: fundamental parameters

## 1 INTRODUCTION

Eclipsing binary stars are one of the most important sources for astrophysics to understand the evolution and the formation of stars. They are valuable variables which may supply the fundamental stellar parameters (e.g. mass and radius) with an accuracy of about 1% (Lacy et al. 2015; Southworth 2013). The orbital parameters of an eclipsing binary system can be obtained by the analysis of radial velocity curve. The orbital inclination and the radii of component stars according to the orbital semi-major axis can only be determined by the light curve analysis of eclipsing binary systems. Therefore, a simultaneous analysis of the high-quality radial velocity and light curves is essential for deriving the fundamental stellar parameters from eclipsing binary stars. Precise fundamental stellar parameters offer us a possibility to investigate the stellar evolution in detail and to test the present evolutionary models.

In a theoretical evolutionary model of a star, mass is a basic parameter. In addition to this parameter, metallicity has also a significant effect on the evolution. Therefore, to calculate an accurate theoretical evolutionary model, it is necessary to obtain a precise value of both mass and metallicity. In the case of double-lined eclipsing binary stars, masses of component stars can be derived from the analysis of light and radial velocity curves, whereas the accurate metallicity parameter can be determined from the spectroscopic analysis of individual spectra of component stars. For this purpose, the spectral disentangling method was developed (Simon & Sturm 1994). This method has been applied by several authors (Pavlovski, Southworth, & Tamajo 2018; Dervişoğlu et al. 2018; Soyduğan et al. 2015, e.g.) to obtain the individual spectra of component stars in double-lined eclipsing binaries. By performing this method, the metallicity value, as well as the atmospheric parameters of each component star can be derived separately.

The most recent eclipsing binary catalogue was published by Avvakumova, Malkov, & Kniazev (2013). The cat-

\* E-mail: filizkahraman01@gmail.com

atalogue consists of 7200 stars including detached, semi-detached and contact binaries. A catalogue for detached double-lined eclipsing binary stars was given by Eker et al. (2014). In this catalogue, they presented the range of effective temperature ( $T_{\text{eff}}$ ), mass ( $M$ ), and radius ( $R$ ) of those eclipsing binaries and showed that for these binaries the accuracy of  $M$  and  $R$  measurements changes from 1% to 5%. Additionally, they pointed out the missing sample of giant and supergiant component stars inside their catalogue. The other catalogue of detached eclipsing binaries is “DEBcat: catalogue of the physical properties of well-studied eclipsing binaries”<sup>1</sup> (Southworth 2015). This catalogue has been available since 2006 and it is a continuation of the list given by Andersen (1991). The catalogue contains precise fundamental stellar parameters ( $M$ ,  $R$ ), surface gravity ( $\log g$ ),  $T_{\text{eff}}$ , luminosity ( $L$ ), and metallicity values of detached systems. The DEBcat is always updated when a new precise measurement of detached eclipsing binaries is presented in the literature.

To improve the stellar evolutionary models and examine the star formation in detail, the double-lined eclipsing binaries, in particular, the detached ones, are very valuable. Therefore, in this study, we focus on an extensive spectroscopic and photometric analysis of three detached eclipsing binary stars, V2080 Cyg, V372 And, and CF Lyn. As these systems have enough archival data, they were selected for this study. All systems were first classified to be variable stars by the Hipparcos (ESA 1997). V2080 Cyg (HIP 95611) has a spectral type of F4V + F4V (Eker et al. 2014). The first detail study of V2080 Cyg was published by Ibanoglu et al. (2008). In this study, they presented a radial velocity and light curve analysis of the binary system and classified it as a double-lined detached eclipsing binary. They also examined the pulsation variability in the component stars, however, no pulsation feature was found. V372 And (HIP 9740) is classified as a main-sequence detached system in the catalogue of eclipsing binary variables (Avvakumova, Malkov, & Kniazev 2013). The star has no detailed analysis in the literature. CF Lyn (HIP 37748) is also classified as a detached eclipsing binary system with a spectral type of F8 in the same eclipsing binary stars catalogue (Avvakumova, Malkov, & Kniazev 2013). The first light curve analysis of CF Lyn was presented by Zasche (2017). No spectroscopic analysis is available for this star.

To derive the fundamental stellar ( $M$ ,  $R$ ), atmospheric parameters ( $T_{\text{eff}}$ ,  $\log g$  and microturbulence velocity  $\xi$ ) and the metallicity of all component stars, we carried out an extensive analysis of the selected eclipsing binary systems. We give the information about the used photometric and spectroscopic data in Sect. 2. The detailed spectroscopic analysis including the radial velocity, spectral disentangling and the determination of atmospheric parameters is introduced in Sect. 3. The light curve analysis of the systems is presented in Sect. 4. The investigation of evolutionary status of the detached eclipsing binaries and an argument about the derived parameters are given in Sect. 5. The conclusions are presented in Sect. 6.

**Table 1.** Information for the selected eclipsing binaries.

Name	V (mag)	SuperWASP Points	ELODIE Spectra	S/N Range
V2080 Cyg	7.90	5858	8	20 - 140
V372 And	9.28	2718	10	25 - 80
CF Lyn	10.05	5461	10	20 - 75

## 2 PHOTOMETRIC AND SPECTROSCOPIC DATA

Photometric and spectroscopic data of the systems were collected from the public databases of the Super Wide Angle Search for Planets (SuperWASP) and ELODIE, respectively.

The SuperWASP is a two-site ground-based programme which aims to discover exoplanets by transit method (Pollacco et al. 2006). The SuperWASP observations have been carried out by the broad-band filters ( $\sim 4000 - 7000 \text{ \AA}$ ) since 2006. In addition to exoplanet discoveries, the SuperWASP has provided data of many variable stars. The selected detached eclipsing binary stars also have the data in the SuperWASP archive<sup>2</sup>. The data of the systems are sufficient for planning photometric analysis. All available data in the database were collected. The scattered points beyond the  $3\sigma$  level were removed for the following analysis. The available data points of the systems in the SuperWASP archive are given in Table 1.

The spectra of the systems were taken from the ELODIE archive<sup>3</sup>. The ELODIE is an échelle spectrograph mounted on the 1.93-m telescope in the observatoire de Haute (France). The spectrograph was used between  $\sim 1993$  and 2006. It provided spectra with a resolving power of 42000 and in a wavelength range of  $\sim 3850$  to  $6800 \text{ \AA}$ . The ELODIE spectra are reduced automatically by the dedicated pipeline. In this study, we used the reduced ELODIE spectra of the systems and normalised them by using the *continuum* task of the NOAO/IRAF<sup>4</sup> package. The number of the available spectra of each binary system and the minimum and maximum signal-to-noise (S/N) ratios of the spectra are given in Table 1.

## 3 SPECTROSCOPIC ANALYSIS

A detailed spectroscopic analysis of the selected systems was planned to carry out to obtain the orbital parameters, the fundamental atmospheric parameters, abundances and the projected rotational velocity ( $v \sin i$ ) values of component stars in each detached eclipsing binary system. Therefore, the analysis of the radial velocity, the spectral disentangling, the atmospheric parameters, and the abundance was performed.

### 3.1 Radial velocity measurements and analysis

To derive the accurate orbital parameters of eclipsing binary systems via the radial velocity analysis, the measured radial velocities of component stars are preferred to be spread

<sup>1</sup> <http://www.astro.keele.ac.uk/jkt/debcat/>

<sup>2</sup> <https://wasp.cerit-sc.cz/form>

<sup>3</sup> <http://atlas.obs-hp.fr/elodie/>

<sup>4</sup> <http://iraf.noao.edu/>

over the orbital phase. In our study, the used spectra offer this property. To obtain the radial velocity ( $v_r$ ) measurements of each component star in the binaries, we used the FXCOR task of the NOAO/IRAF package program. In the measurements, the radial velocity standard star HD 50692 ( $v_r = -15.5 \text{ km s}^{-1}$ , Udry, Mayor, & Queloz 1999) was used as a template. During the analysis, the spectra having the lowest S/N ratio in each system were excluded. The obtained  $v_r$  measurements are given in Table A1.

We derived the orbital parameters, eccentricity  $e$ , argument of periastron  $\omega$ , the velocity of the system mass center  $V\gamma$ , mass ratio  $q$  ( $M_{\text{secondary}}/M_{\text{primary}}$ ),  $a \sin i$  ( $a$  is semi-major axis and  $i$  is inclination), and the amplitude of the  $v_r$  curve of the star with respect to the center of mass of the binary  $K$  by analysing the determined  $v_r$  curves of the systems. In the analysis, we used the `rvfit` code<sup>5</sup>. The `rvfit` code fits the  $v_r$  curves of double-lined, single-lined binaries or exoplanets by using a minimization method of adaptive simulated annealing (Iglesias-Marzoa, López-Morales, & Jesús Arévalo Morales 2015). It is a user-friendly code which automatically fits the given orbital parameters above, the orbital period  $P$  and also the periastron passage time  $T_p$ .

In the  $v_r$  analysis, the  $P$  and  $T_p$  parameters of the binaries were kept fixed and they were taken from Kreiner (2004). In the analysis of V2080 Cyg, we also used the previously obtained  $v_r$  measurements by Ibanoglu et al. (2008). As a result of the analysis, the orbital parameters were derived and it was found that V2080 Cyg and V372 And have a circular orbit, whereas CF Lyn has an eccentric orbit with a value of about 0.03. The uncertainties of the obtained result were calculated using the Markov Chain Monte Carlo method. The results are listed in Table 2. The theoretical  $v_r$  curves fit to the obtained  $v_r$  measurements and the difference between them are shown in Fig. 1.

### 3.2 Spectral disentangling

For the investigation of the evolutionary status of each component star in the selected detached eclipsing binaries, the metallicity values are needed to be known. However, the spectra of the systems are composite. Therefore, to obtain the spectra of individual component stars in the binaries, we applied the spectral disentangling method. The `FDBINARY` code (Ilijic et al. 2004) was used in the analysis. The `FDBINARY` disentangles a composite spectrum in the Fourier space. It is also capable of resolving the third component spectrum. To apply the disentangling method via the `FDBINARY` first light contributions of component stars in total should be known. Therefore, we first carried out a preliminary light curve analysis by assuming the primary component stars'  $T_{\text{eff}}$  values from their spectral type. In this assumption, the spectral type –  $T_{\text{eff}}$  relation given by Gray & Corbally (2009) was used. As a result of this preliminary analysis, we obtained the light contributions of each component star in total. It turned out that V372 And and CF Lyn are two-body systems, while V2080 Cyg has a third component. Approximately, the light contributions of the primary and secondary components were found to be 77%

and 23% for V372 And, 94% and 6% for CF Lyn. The light contributions of the primary, secondary and third components of V2080 Cyg were also obtained about 52%, 40%, and 8%, respectively. The updated light curve analysis will be given in Sect. 4.

In the application of the spectral disentangling method, we used the spectral interval of 4000–5500 Å. This spectral interval was divided into ten parts with 100–150 Å steps, and each part was analysed separately. In the analysis, the spectra having the lowest S/N ratios were not used. The derived orbital parameters were used as inputs. The values of  $P$  and  $\omega$  were fixed, while  $T_p$ ,  $K_1$ ,  $K_2$ , and  $e$  were kept as free parameters in the analysis. After the disentangled spectra of each spectral part were obtained, they were re-normalised considering the light ratio of components obtained from the initial light curve analysis. In this process, the procedure given by Ilijic et al. (2004) was used.

As a result of this analysis, a disentangled spectrum with a higher S/N ratio than the average S/N ratio of the input spectra can be obtained (Pavlovski & Southworth 2009). The final S/N ratios of the disentangled spectra of each star were calculated by using the given equation by Pavlovski & Southworth (2009). The final S/N ratios for the primary, secondary and the third components of V2080 Cyg were found to be 135, 103 and 21, respectively. For V372 And, those values were calculated as 157 for primary and 50 for secondary components. The final S/N values were also obtained to be 140 and 9 for the primary and secondary components of CF Lyn. As can be seen from the result of S/N ratios, except for the third component of V2080 Cyg and the secondary component of CF Lyn, all disentangled spectra are sufficient for the atmospheric parameter determination. Additionally, they are good enough for the abundance analysis. Only the secondary component of V372 And could give results with higher errors because of its lower S/N ratio.

### 3.3 Determination of the atmospheric parameters and the chemical abundances of component stars

The disentangled spectra of each component star were analysed to determine the atmospheric parameters and the abundances of the stars. Before the determination of element abundances, accurate atmospheric parameters should be obtained. Therefore, we first derived the fundamental atmospheric parameters  $T_{\text{eff}}$ ,  $\log g$ ,  $\xi$ , and also  $v \sin i$  values of each component star.

In this analysis, we used the plane-parallel, hydrostatic, line-blanketed local thermodynamic equilibrium (LTE) ATLAS9 model atmospheres (Kurucz 1993). The theoretical spectra were synthesized with the `SYNTH` code (Kurucz & Avrett 1981).

We first determined the initial  $T_{\text{eff}}$  values of the component stars from the H $\beta$  line analysis. Before starting the analysis, we checked the normalisation of H $\beta$  lines by comparing them with synthetic spectra, as these broad lines are affected by the échelle orders merging. If necessary a re-

<sup>5</sup> <http://www.cefca.es/people/riglesias/rvfit.html>

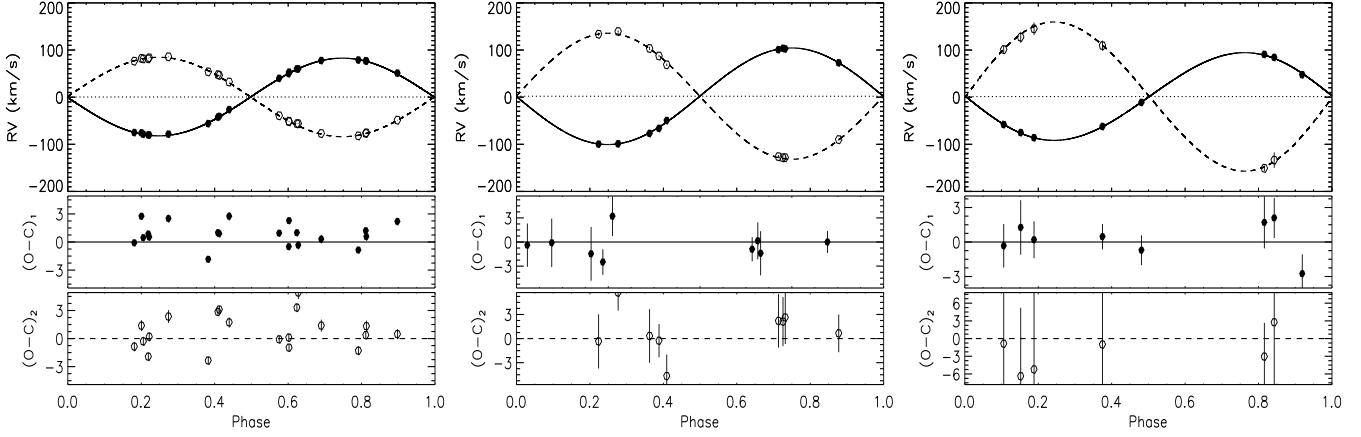


**Figure 1.** The theoretical  $v_r$  curves fit for the measured  $v_r$  values (upper panels) and the residuals (O-C) in  $\text{km s}^{-1}$  (lower panels). The left, middle and right panels belong to V2080 Cyg, V372 And, and CF Lyn, respectively. The subscripts 1 and 2 represent the primary and the secondary components, respectively.

**Table 2.** The results of the radial velocity analysis. The subscripts 1 and 2 represent the primary and the secondary components, respectively. <sup>a</sup> shows the fixed parameters.

Parameter	V2080 Cyg	V372 And	CF Lyn
$T_p$ (HJD) <sup>a</sup>	2452504.186	2452501.191	2452500.070
$P$ (d) <sup>a</sup>	4.9335660	2.9410200	1.3853720
$\gamma$ (km/s)	$1.07 \pm 0.07$	$1.96 \pm 0.54$	$1.36 \pm 0.73$
$K_1$ (km/s)	$82.35 \pm 0.10$	$102.43 \pm 0.95$	$93.03 \pm 1.15$
$K_2$ (km/s)	$83.99 \pm 0.16$	$133.72 \pm 1.21$	$158.22 \pm 4.68$
$e$	$0.000 \pm 0.001$	$0.000 \pm 0.004$	$0.030 \pm 0.009$
$\omega$ (deg)	$90.63 \pm 0.07$	$90.23 \pm 0.62$	$89.09 \pm 0.58$
$a_1 \sin i$ ( $10^6$ km)	$5.587 \pm 0.007$	$4.142 \pm 0.038$	$1.771 \pm 0.022$
$a_2 \sin i$ ( $10^6$ km)	$5.698 \pm 0.011$	$5.408 \pm 0.049$	$3.013 \pm 0.089$
$a \sin i$ ( $10^6$ km)	$11.285 \pm 0.013$	$9.550 \pm 0.062$	$4.784 \pm 0.091$
$M_1 \sin^3 i$ ( $M_\odot$ )	$1.188 \pm 0.005$	$2.272 \pm 0.048$	$1.432 \pm 0.097$
$M_2 \sin^3 i$ ( $M_\odot$ )	$1.165 \pm 0.003$	$1.740 \pm 0.035$	$0.842 \pm 0.036$
$q = M_2/M_1$	$0.980 \pm 0.002$	$0.766 \pm 0.010$	$0.588 \pm 0.019$

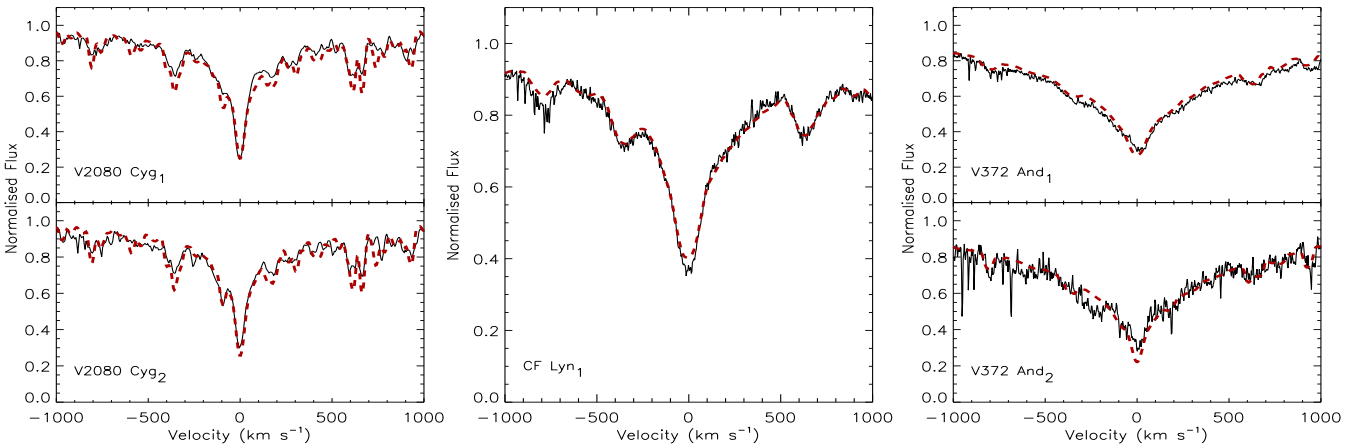


**Figure 2.** Comparison of the theoretical (dashed line) and disentangled  $H_\beta$  lines (continuous line) of component stars. The subscripts 1 and 2 represent the primary and the secondary components, respectively.



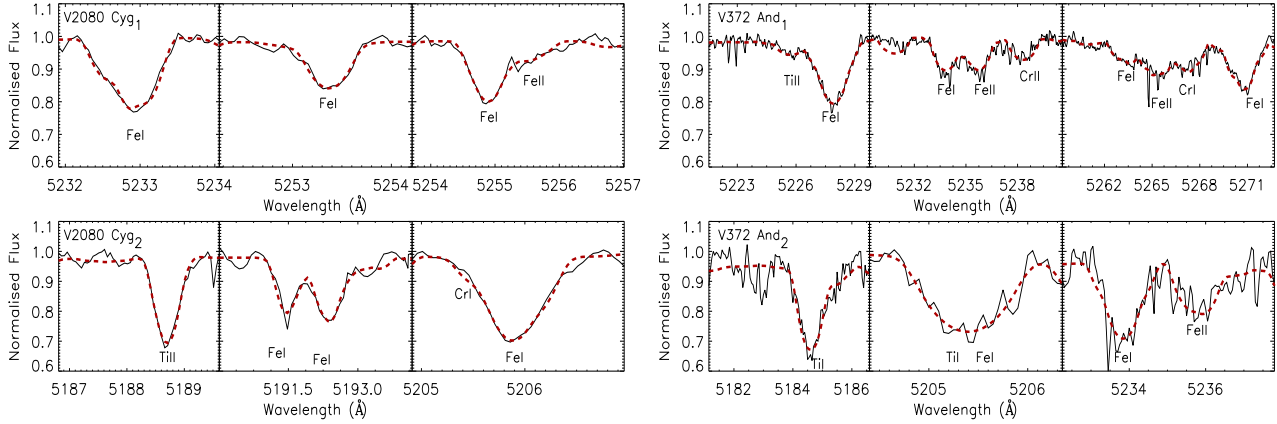


**Figure 3.** Comparison of the theoretical (dashed lines) and disentangled spectra (continuous lines) of component stars of V2080 Cyg (left panels) and V372 And (right panels). The subscripts 1 and 2 represent the primary and the secondary components, respectively. A similar figure for CF Lyn is given in Fig. A1

normalisation process was applied with the *continuum* task of the NOAO/IRAF package<sup>6</sup>.

In the  $H\beta$  line analysis, the  $T_{\text{eff}}$  values were obtained considering the minimization method (Catanzaro, Leone, & Dall 2004). During the analysis, the metallicity and  $\log g$  parameters were assumed to be solar and 4.0 cgs, respectively. The resulting  $H\beta$   $T_{\text{eff}}$  values were determined taking into account the minimum difference between the synthetic and observed spectra. The uncertainties in  $T_{\text{eff}}$  values were estimated considering the  $1\sigma$  change in the difference between the observed and synthetic spectra and also taking 100 K error introduced by normalisation. The results of the analysis are given in Table 3. A comparison between the theoretical and disentangled  $H\beta$  lines is shown in Fig. 2.

Final atmospheric parameters were determined based on the excitation and the ionization equilibrium of iron (Fe) lines. This is because for the accurate atmospheric parameters, the abundance of an element obtained from different excitation or ionization potential must be the same.

The disentangled spectra of the component stars were divided into small spectral parts considering the normalisation level. The line identification of each spectral part was made by using the Kurucz line list<sup>7</sup>. In the analysis, we used the spectrum synthesis method which generates the theoretical spectrum until it fits well the observed one. In the analysis, each spectral part was analysed separately.

$T_{\text{eff}}$  and  $\xi$  parameters sensitively depend on the strength of Fe I lines, while they show no significant dependence on Fe II lines. On the contrary,  $\log g$  parameter is very sensitive to the strength of Fe II lines. Therefore, the  $T_{\text{eff}}$  values of the component stars were determined by considering the correlation between Fe I abundance and the excitation potential. Additionally, the  $\xi$  parameters were derived by checking the relation between the depth of Fe I lines and abundances. The  $\log g$  values were also derived relying on the relationship between the

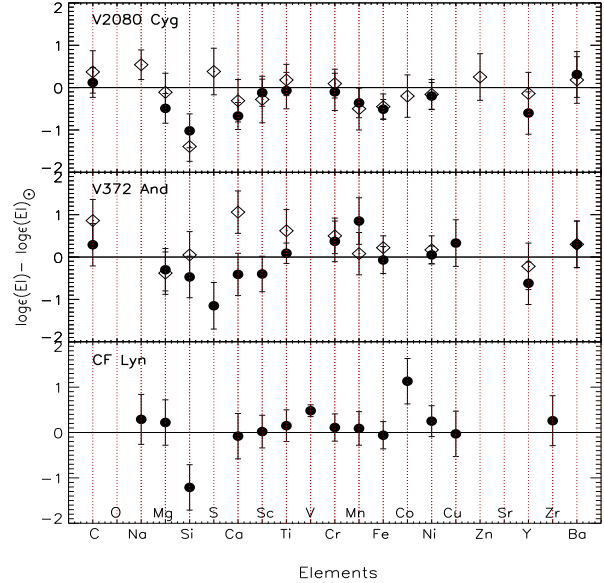


**Figure 4.** Chemical abundances distribution of stars relative to the solar values (Asplund et al. 2009). The filled circle and diamond symbols represent the primary and the secondary components, respectively.

ionization balance and abundances of Fe II (for more information see Kahraman Alicağuş et al. 2016). The  $v \sin i$  values were also determined during the analysis. To estimate the errors in the  $T_{\text{eff}}$ ,  $\log g$  and  $\xi$ , we took into account  $\sim 5\%$  changes in the relationships of the excitation potential–abundance, the ionization potential–abundance and the line depth–abundance, respectively. The derived final atmospheric parameters and the  $v \sin i$  values of each component stars are given in Table 3. The atmospheric parameters of the second and third components of CF Lyn and V2080 Cyg could not be derived because of their low S/N ratio disentangled spectra.

After the accurate atmospheric parameters were derived, we performed the abundance analysis by taking these

<sup>6</sup> <http://iraf.noao.edu/>

<sup>7</sup> [kurucz.harvard.edu/linelists.html](http://kurucz.harvard.edu/linelists.html)

**Table 3.** The  $H\beta$   $T_{\text{eff}}$  values, the final atmospheric parameters,  $v \sin i$  and the Fe abundances of the component stars. The subscripts 1 and 2 represent the primary and the secondary components, respectively.

Star	$H\beta$ line	Fe lines				
	$T_{\text{eff}}$ (K)	$T_{\text{eff}}$ (K)	$\log g$ (cgs)	$\xi$ (km s $^{-1}$ )	$v \sin i$ (km s $^{-1}$ )	$\log \epsilon$ (Fe)
V2080 Cyg <sub>1</sub>	6200 $\pm$ 200	6100 $\pm$ 100	4.0 $\pm$ 0.1	1.8 $\pm$ 0.2	23 $\pm$ 3	6.99 $\pm$ 0.25
V2080 Cyg <sub>2</sub>	6100 $\pm$ 300	6300 $\pm$ 200	4.2 $\pm$ 0.1	2.1 $\pm$ 0.2	22 $\pm$ 3	7.17 $\pm$ 0.29
V372 And <sub>1</sub>	7900 $\pm$ 200	8000 $\pm$ 100	3.9 $\pm$ 0.1	2.4 $\pm$ 0.2	56 $\pm$ 4	7.43 $\pm$ 0.25
V372 And <sub>2</sub>	7800 $\pm$ 300	7800 $\pm$ 200	4.2 $\pm$ 0.2	2.7 $\pm$ 0.3	33 $\pm$ 3	7.72 $\pm$ 0.33
CF Lyn <sub>1</sub>	6200 $\pm$ 300	6600 $\pm$ 200	4.0 $\pm$ 0.1	2.3 $\pm$ 0.3	82 $\pm$ 5	7.44 $\pm$ 0.26

parameters fixed. The abundances were derived by using the spectrum synthesis method which is more suitable for the analysis of stars having slow to high  $v \sin i$  values. The line-identified spectral parts were analysed separately. The final element abundances were determined by adjusting the abundances of individual elements and considering the minimum difference between the observed and synthetic spectra. After the analysis of each spectral parts of individual stars, the average values of the calculated element abundances were obtained. The obtained theoretical spectra fits for the observed lines of the components of V2080 Cyg and V372 And are shown in Fig. 3.

There are a few quantities which affect the uncertainties of chemical element abundances. The assumption in model atmosphere calculations, quality of observed spectra (S/N and resolution), error in determined atmospheric parameters are significant uncertainty sources. To estimate the real error in the derived chemical abundances, we checked the uncertainty effects of those sources. It was calculated that the assumptions (local thermodynamical equilibrium, plane-parallel geometry, and hydrostatic equilibrium) in model atmosphere contribute about 0.1 dex error in abundances (Mashonkina 2011). The quality effect of a spectrum was examined by Kahraman Aliçavuş et al. (2016). We took the uncertainty contribution of this effect from this study. Additionally, we calculated by how much chemical abundance is changed with 100 K difference in  $T_{\text{eff}}$ , 0.1 cgs variation in  $\log g$ , and 0.1 km s $^{-1}$  in  $\xi$ . It turned out that the variations in  $T_{\text{eff}}$  and  $\xi$  make around 0.08 dex difference in abundance. The  $\log g$  error contribution was also found  $\sim$ 0.05 dex. Those results are similar to the errors found by Kahraman Aliçavuş et al. (2016). The resulting uncertainties for the elements were calculated considering all error contributions. The Fe line abundance and a list of the element abundances of each component star are given in Table 3 and Table A2, respectively. In Table A2, the number of analysed spectral parts is given in the brackets. As can be noticed, abundance values for some elements were obtained from less number of spectral parts. Therefore, it should be kept in mind that these abundances are not so reliable. The abundance distributions of component stars relative to solar abundance are shown in Fig. 4.

As a result of this analysis, we found that the components of V2080 Cyg show slightly lower Fe abundance comparing to solar abundance (Asplund et al. 2009). The primary component of V2080 Cyg has a lower Fe abundance relative to the secondary component but those Fe abundances agree with each other within the uncertainties. Additionally, it turned out that the component stars of V372 And and CF Lyn have element abundances similar to solar within the errors.

## 4 LIGHT-CURVE SOLUTION

The normalised SuperWASP data of the eclipsing binary systems was used in the light curve analysis. To obtain more accurate results the SuperWASP data and the measured  $v_r$  values were analysed simultaneously by using the Wilson–Devinney code (Wilson & Devinney 1971) combined with the Monte Carlo simulation to calculate the uncertainties of the searched parameters (Zola et al. 2010, 2004). The light curves of the systems are good enough for this analysis. Only V2080 Cyg has a lack of descending branch in the primary minimum. However, there are enough data points to fit the primary eclipse.

Final  $T_{\text{eff}}$  values of the primary components were fixed during the analysis. The bolometric albedos (Ruciński 1969) and the bolometric gravity-darkening coefficients (von Zeipel 1924) were set to be 1 for radiative atmospheres. They were also set as 0.5 and 0.32 for convective atmospheres, respectively. The logarithmic limb darkening coefficients were taken from van Hamme (1993) and they were also fixed during the analysis. Additionally, a synchronous rotation was assumed. The  $T_{\text{eff}}$  values of secondary components, phase shift ( $\phi$ ),  $i$ ,  $q$ , and fractional luminosities, dimensionless potentials ( $\Omega$ ) of component stars were set as free parameters. The derived orbital parameters from  $v_r$  analysis were used as input values. During the analysis, a detached binary configuration was assumed. Additionally, we set the third light contribution as a free parameter.

Consequently, we determined the final parameters of the binary systems and a third light contribution was found for V2080 Cyg. Additionally, the astrophysical parameters of each component star were calculated by the JKTEB-SDIM code (Southworth, Maxted, & Smalley 2004) which carefully estimates the uncertainties in the derived fundamental parameters. The distances of the binary systems were also determined by utilizing the distance modulus. To calculate the distances, the bolometric correction and the absorption values were taken from Eker et al. (2018) and Schlafly & Finkbeiner (2011), respectively. Final orbital parameters and the derived parameters are listed in Table 4. The theoretical light curves' fit to the SuperWASP light curves is demonstrated in Fig. 5.

## 5 DISCUSSION

### 5.1 Fundamental properties

As a result of the analysis of the light and radial velocity curves, the fundamental stellar parameters,  $L$  and  $M_{\text{bolometric}}$  values of all component stars were obtained. The accuracy of the  $M$  and  $R$  values ranges between 1% and

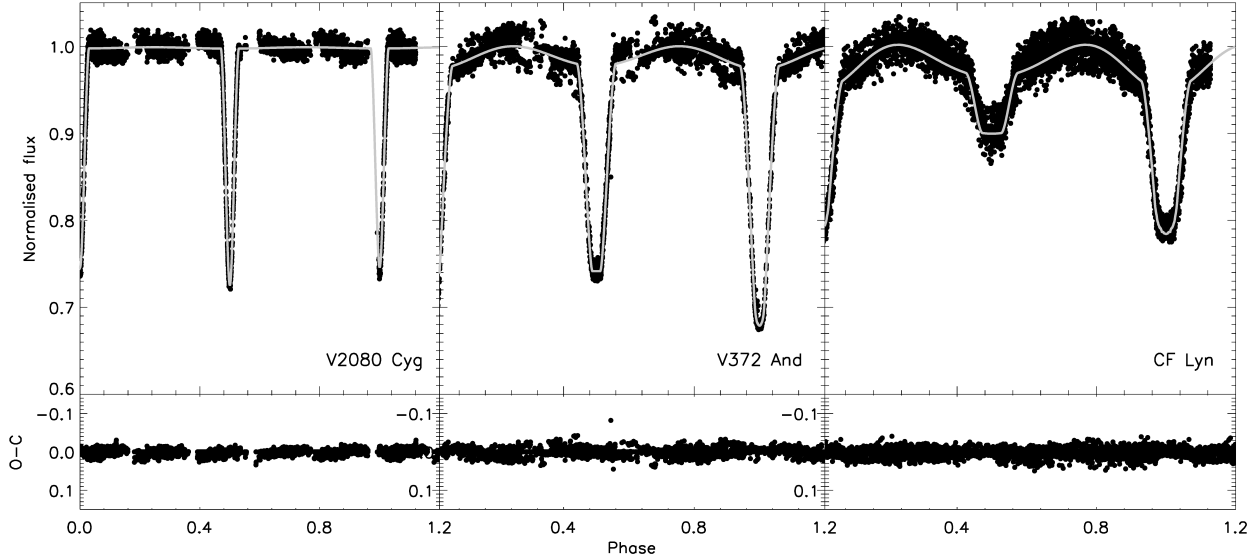


Figure 5. Upper panel: comparison of observed (dots) and theoretical light curves (solid line). Lower panel: residuals.

Table 4. Results of the light curve analysis and the astrophysical parameters. The subscripts 1, 2 and 3 represent the primary, the secondary, and third components, respectively. <sup>a</sup> shows the fixed parameters.

Parameter	V2080 Cyg	V372 And	CF Lyn
$i$ ( $^{\circ}$ )	$86.009 \pm 0.091$	$86.947 \pm 0.209$	$83.818 \pm 0.210$
$T_{\text{eff}1}^a$ (K)	$6100 \pm 100$	$8000 \pm 100$	$6600 \pm 200$
$T_{\text{eff}2}$ (K)	$6210 \pm 250$	$7620 \pm 340$	$5220 \pm 260$
$V_{\gamma}$ ( $\text{km s}^{-1}$ )	$1.170 \pm 0.321$	$-2.490 \pm 0.003$	$1.364 \pm 0.051$
$a$ ( $R_{\odot}$ )	$16.254 \pm 0.019$	$13.742 \pm 0.090$	$6.912 \pm 0.132$
$e$	$0^a$	$0^a$	$0.029 \pm 0.003$
$\Omega_1$	$10.339 \pm 0.179$	$5.133 \pm 0.017$	$3.732 \pm 0.010$
$\Omega_2$	$11.925 \pm 0.242$	$6.755 \pm 0.038$	$5.686 \pm 0.024$
Phase shift	$0.00001 \pm 0.00001$	$0.00011 \pm 0.00009$	$0.00100 \pm 0.00010$
$q$	$0.982 \pm 0.002$	$0.775 \pm 0.004$	$0.586 \pm 0.003$
$r_1^*$ (mean)	$0.1067 \pm 0.0019$	$0.2306 \pm 0.0010$	$0.3250 \pm 0.0023$
$r_2^*$ (mean)	$0.0898 \pm 0.0018$	$0.1373 \pm 0.0009$	$0.1316 \pm 0.00107$
$L_1 / (L_1 + L_2)$	$0.568 \pm 0.024$	$0.767 \pm 0.010$	$0.943 \pm 0.009$
$L_2 / (L_1 + L_2)$	$0.432 \pm 0.020$	$0.233 \pm 0.009$	$0.057 \pm 0.009$
$l_3$	$0.083 \pm 0.015$		
Derived Quantities			
$M_1$ ( $M_{\odot}$ )	$1.197 \pm 0.005$	$2.282 \pm 0.048$	$1.457 \pm 0.099$
$M_2$ ( $M_{\odot}$ )	$1.173 \pm 0.004$	$1.748 \pm 0.035$	$0.857 \pm 0.037$
$R_1$ ( $R_{\odot}$ )	$1.734 \pm 0.031$	$3.170 \pm 0.025$	$2.247 \pm 0.046$
$R_2$ ( $R_{\odot}$ )	$1.459 \pm 0.029$	$1.887 \pm 0.017$	$0.909 \pm 0.021$
$\log L_1$ ( $L_{\odot}$ )	$0.575 \pm 0.032$	$1.570 \pm 0.023$	$0.937 \pm 0.056$
$\log L_2$ ( $L_{\odot}$ )	$0.457 \pm 0.072$	$1.034 \pm 0.078$	$-0.257 \pm 0.088$
$\log g_1$ (cgs)	$4.038 \pm 0.016$	$3.794 \pm 0.005$	$3.898 \pm 0.014$
$\log g_2$ (cgs)	$4.179 \pm 0.017$	$4.129 \pm 0.007$	$4.453 \pm 0.009$
$M_{\text{bolometric}1}$ (mag)	$3.313 \pm 0.081$	$0.825 \pm 0.057$	$2.408 \pm 0.139$
$M_{\text{bolometric}2}$ (mag)	$3.608 \pm 0.180$	$2.165 \pm 0.195$	$5.394 \pm 0.221$
Distance (pc)	$86 \pm 4$	$472 \pm 29$	$231 \pm 17$

\*fractional radius,  $R/a$ .

2% for V2080 Cyg and V372 And. However, the accuracy of these parameters reaches 4 – 6% for  $M$  and  $\sim 2\%$  for  $R$  in CF Lyn case. As CF Lyn has an eccentric orbit, the error in the determined parameters come higher comparing the other systems. To decrease these error bars, new spectroscopic data taken from whole orbital phases is necessary. When

the accuracy criteria given by Eker et al. (2018) is considered, the derived fundamental parameters of V2080 Cyg and V372 And are very accurate ( $M$  and  $R$  uncertainties  $\leq 3\%$ ) and these obtained parameters are accurate ( $M$  and  $R$  uncertainties 3–6%) for CF Lyn. The distances of systems were calculated to be  $472 \pm 29$ ,  $231 \pm 17$ , and  $86 \pm 4$  pc for

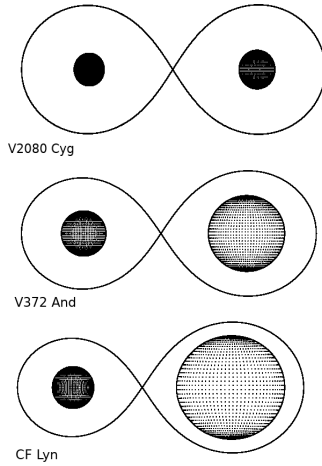


**Figure 6.** Roche geometries of the detached systems at orbital phase 0.75.

V372 And, CF Lyn, and V2080 Cyg, respectively. These distance values were found to be consistent with the distance values given by Gaia (Gaia Collaboration et al. 2018).

A synchronous rotation was assumed in the light curve analysis. Therefore, the rotation period of the component stars should be the same with the orbital period of binary system. Using this approach and the derived radii of the component stars, we can calculate the synchronous  $v \sin i$  parameters of components. The synchronous  $v \sin i$  values of the primary and the secondary components of CF Lyn were found to be 81 and 37  $\text{km s}^{-1}$ , respectively. As we only obtained the good quality disentangled spectrum of the primary component of CF Lyn, only the  $v \sin i$  value of the primary component star was derived from the spectroscopic analysis. The synchronous and the spectroscopic  $v \sin i$  values of CF Lyn are consistent with each other. For the primary and secondary components of V372 And, the synchronous  $v \sin i$  values were calculated as 55 and 36  $\text{km s}^{-1}$ . These values also agree with the spectroscopic  $v \sin i$  within the errors. The synchronous  $v \sin i$  values of the primary and secondary components of V2080 Cyg were also obtained as 18 and 15  $\text{km s}^{-1}$ , respectively. These values are slightly different than the spectroscopic  $v \sin i$  values. This difference can be caused by the effect of the third component.

In previous studies, it was indicated that an evolution from detached to semi-detached binaries and also from semi-detached to contact binaries exist (Stępień & Gazeas 2012; Yakut & Eggleton 2005, e.g.). Particularly, the detached systems having the  $q$  value lower than average (the average  $q$  value is  $\sim 0.9$ , Eker et al. 2014) are good candidates to examine the evolution from detached to semi-detached binaries. In our sample, the detached binary systems have different  $q$  values. The  $q$  values are about 0.78, 0.98 and 0.59 for V372 And, V2080 Cyg and CF Lyn, respectively. We calculated the Roche lobe filling factor<sup>8</sup> of each component star to see how much they fill their Roche lobes. It turned out that the primary and secondary components of V2080 Cyg have a filling factor of 37% and 32%, respectively. The fill-

ing factor value for the primary component of V372 And was found as 67% and for the secondary component, it was obtained as 51%. Furthermore, we found that the primary and secondary components of CF Lyn fill their Roche lobes in a ratio of 80% and 54%, respectively. The Roche geometries of the detached binary systems are illustrated in Fig. 6. For detached binary systems, it was shown that the component stars having the filling factor value  $> 75\%$  exhibit non-spherical shapes (Eker et al. 2014). As demonstrated in Fig. 6, CF Lyn also shows a non-spherical shape.

## 5.2 Atmospheric parameters and chemical composition

Using the disentangled spectra of component stars, we derived their fundamental atmospheric parameters,  $v \sin i$  values and the chemical compositions by applying the spectrum synthesis method. The  $T_{\text{eff}}$  values of components were determined from  $\text{H}\beta$  and Fe lines. The obtained  $T_{\text{eff}}$  value of V2080 Cyg is consistent with the assumed  $T_{\text{eff}}$  used in previous light curve analysis (İbanoglu et al. 2008). The  $\log g$  values were also calculated using the derived parameters from the light curve analysis and those values were found to be consistent with the spectroscopic  $\log g$  values within the errors.

The element abundances were determined as well. The Fe abundances of each component stars are given in Table 3. As can be seen from the table, the components of CF Lyn and V372 And have Fe abundance similar to solar (7.50 dex). We found that the components of V2080 Cyg show slightly lower Fe abundance comparing to solar and they have similar Fe abundance within the error bars which is expected in the theory since the binary stars are assumed to form in the same interstellar area. We also found that the secondary component of V2080 Cyg is slightly hotter than the primary one.

## 5.3 Evolutionary models

The evolutionary models of the analysed detached binary systems were computed by using the Modules for Experiments in Stellar Astrophysics (MESA) evolution code (Paxton et al. 2011, 2013). MESA includes a binary module (Paxton et al. 2015) for simulating the binary orbital evolution and finding the initial parameters of binary systems.

We calculated many evolutionary models for different starting parameters using the MESA. The metallicity ( $Z$ ) parameters was taken as 0.02 for examining the evolutionary status of the components of CF Lyn and V372 And. Because when the error bars in the Fe abundances of individual components are taken into account (see, Table 3), except for the components of V2080 Cyg, the other components have Fe abundance similar to solar. The components of V2080 Cyg have slightly lower Fe abundance. As binary stars are assumed to form in the same environment, we determined the same  $Z$  value of 0.017 for the components of V2080 Cyg from the best fit evolutionary model. Evolutionary models were analysed by comparing the  $R$  and  $\log g$  values of the component stars. During the analysis, orbital period and eccentricity ( $e$ ) planes were investigated for CF Lyn as it has an eccentric orbit. Additionally, the obtained fundamental stellar parameters of each component star were used as initial

<sup>8</sup> Filling factor =  $(\Omega_{\text{inner}} - \Omega) / (\Omega_{\text{outer}} - \Omega_{\text{inner}})$



**Table 5.** Results obtained from the best-fit evolutionary models. Assumed parameters are illustrated by \* symbol.

Parameter	V2080 Cyg	V372 And	CF Lyn
$P_{\text{initial}}$ (days)	5.17 (25)	3.20 (8)	3.40 (10)
$v_{1\text{initial}}$ (km s $^{-1}$ )	24 (5)	175 (25)	112 (15)
$v_{2\text{initial}}$ (km s $^{-1}$ )	22 (5)	37 (8)	10 (7)
$e_{\text{initial}}$	0*	0*	0.53 (5)
Age (Gyr)	3.95 (20)	0.58 (4)	2.00 (20)

parameters in the analysis. As a result, the most probable ages were determined and the orbital evolution scenarios were produced for each system. The best-fit evolutionary tracks and the position of each component star in the examined binary systems are shown in Fig. 7. The positions of the stars in the Age– $\log R$  diagram are also illustrated in Fig. 8. The result of evolutionary models of the binary systems is given in Table 5.

For V2080 Cyg, we obtained a younger age comparing the age value given by Ibanoglu et al. (2008). Additionally, in all calculated evolutionary models for V2080 Cyg, we found that the system should show a synchronous rotation. However, the obtained spectroscopic  $v \sin i$  values indicate that the observed situation is different. This difference can be caused by the effect of third body in the binary system of V2080 Cyg. When the obtained results for V372 And are examined, it is clear that the primary component needs to start its evolution with a very high initial  $v \sin i$  values. For CF Lyn system, it was found that the  $e$  should start at a very high value like 0.53 in the beginning of the evolution in order to be able to adhere to the present age of the system. However, precise light curve observations are needed to examine this situation more clearly.

The components of V2080 Cyg and V372 And also show consistency with the models illustrated in the Age– $\log R$  diagram. However, the secondary component of CF Lyn differs from the model, while primary star is consistent with the model within the errors. The obtained radius of the small mass component of CF Lyn is considerably larger than the predicted values from the models. The most likely explanation for this situation may be the result of the magnetic activity of the small mass component (Torres, Vaz, & Sandberg Lacy 2008; Stassun et al. 2009). In addition to the the magnetic activity, the other factor can be the possibility of periodic mass transfer between the components as a result of the evolution of the orbit which started with a high degree of eccentricity. This may cause the discrepancy in the surface abundance and the radius of the low mass component.

## 6 CONCLUSIONS

In this study, a detailed examination of three double-lined detached eclipsing binary systems is presented. We first carried out a radial velocity and light curve analysis and derived the accurate fundamental stellar parameters of the systems. The Roche geometries and the filling factors were examined using the derived stellar parameters. It turned out that the primary component of CF Lyn fills 80% of its Roche lobe and it has a non-spherical shape. CF Lyn can be a good candi-

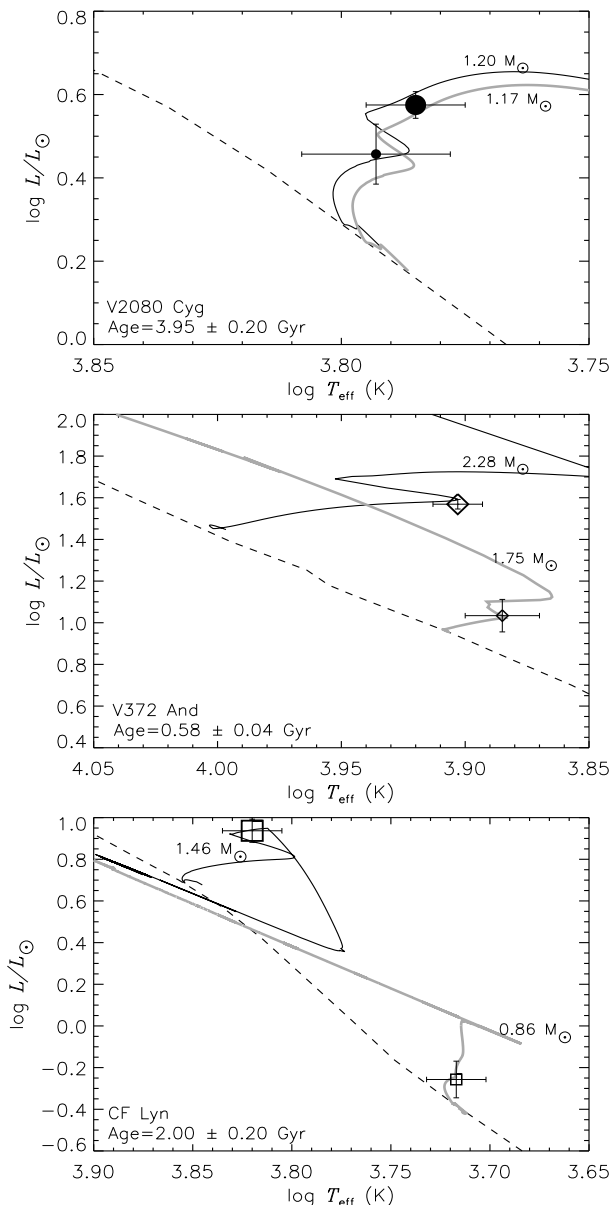


**Figure 7.** Position of the primary and the secondary (smaller symbols) component stars on the Hertzsprung-Russell diagram. Dashed line represents the zero age main sequence (ZAMS). The evolutionary tracks are showed by the solid black and gray lines for the primary and secondary stars, respectively. The  $Z$  value is 0.02 for CF Lyn and V372 And, while it is 0.017 for V2080 Cyg.

date system to investigate the evolution between detached to semi-detached binaries.

The atmospheric parameters,  $v \sin i$ , and the abundances of each component star were determined by using the disentangled spectra of the individual systems. As a result, we found a similar  $T_{\text{eff}}$  values from the H $\beta$  and Fe lines analysis within the error bars. The spectroscopic  $\log g$  values were also found to be consistent with the  $\log g$  values calculated from the stellar parameters. All component stars have a moderate  $v \sin i$  value which ranges from 21 to 82 km s $^{-1}$ . Additionally, the spectroscopic  $v \sin i$  values were found to agree with the synchronous  $v \sin i$  value for CF Lyn and V372 And. However, in the case of V2080 Cyg,

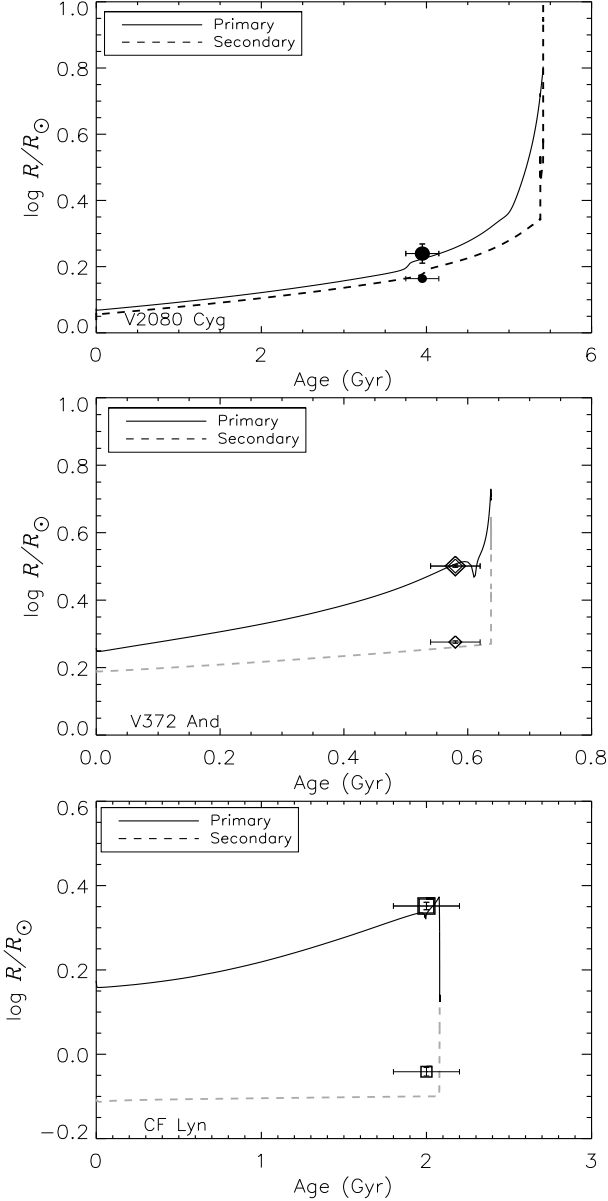


**Figure 8.** Position of the primary and the secondary (smaller symbol) component stars in the Age– $\log R$  diagram. The tracks are showed by the solid black and gray lines for the primary and secondary (smaller symbols) stars, respectively. The  $Z$  value is 0.02 for CF Lyn and V372 And, while it is 0.017 for V2080 Cyg.

they differ from each other. This difference can be explained by the effect of the third component present in the system.

The chemical compositions of the components were derived. The Fe abundance of CF Lyn and V372 And component stars were obtained similar to solar within the errors. However, we found that the components of V2080 Cyg have a lower Fe abundance ( $\lesssim 0.45$  dex) comparing to the solar value.

The evolutionary status of component stars were examined with the binary evolutionary models and the ages of the systems were determined. The components of V2080 Cyg fit well with  $Z = 0.017$  models within the error bars. In the binary evolutionary models of V2080 Cyg, we found that the synchronous rotation should have happened before the

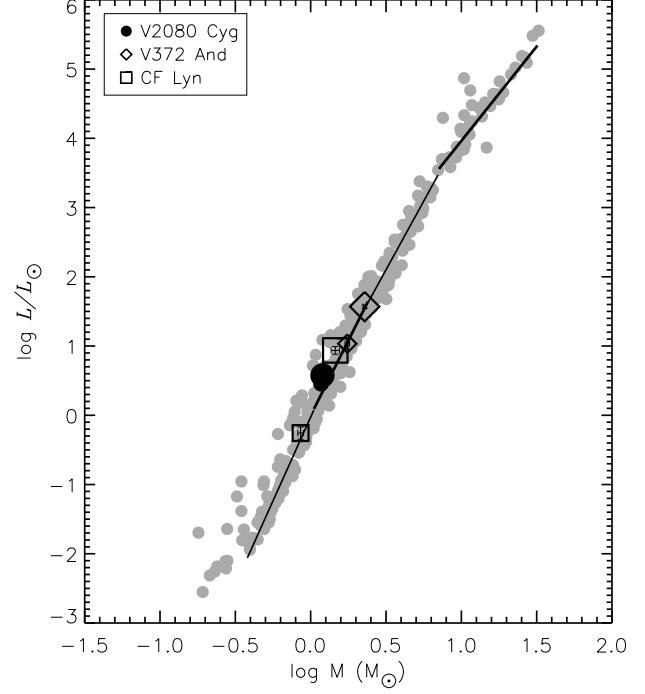


**Figure 9.** The position of the primary and the secondary (smaller symbols) component stars in the the  $\log L - \log M$  diagram. Gray circles represent the double-lined detached eclipsing binaries given by Eker et al. (2014). The solid lines illustrate the relationships between the  $L$  and  $M$  (Eker et al. 2014).

determined age. To explain this difference between the obtained result and the model, it is necessary to determine the properties of the third component and investigate the orbital evolution with n-body simulations.

CF Lyn is an interesting target with an eccentric orbit. A possible explanation for the current eccentricity of CF Lyn is may be the disruption of the orbital dynamics of the binary system by the Kozai mechanism of an invisible third body. It was also found that the dynamic and model predicted radii of the secondary component of CF Lyn differ from each other. This situation can be explained by a possible magnetic activity of the star. For investigating such situation, we need a long-term precise light curve and high-resolution spectra with high S/N ratios.

In Fig. 9, the position of the examined detached eclipsing binaries is shown in the  $\log L - \log M$  diagram with the given double-lined detached eclipsing binary systems by Eker et al. (2014). The relationship between the  $L$  and  $M$  of detached binaries was expressed in four different regions taking into account the mass range (Eker et al. 2014). These relationships are also demonstrated in Fig. 9. As can be seen from the figure, V2080 Cyg, CF Lyn and V372 And are consistent with the given correlations.

We also examined whether the component stars exhibit pulsation or not. By removing the binarity effect from the light curves a frequency analysis was performed using the Period04 (Lenz & Breger 2005). No significant result was found. However, the light curves of the systems are not good enough to find a pulsation variability. In near future, the systems will be observed by The Transiting Exoplanet Survey

Satellite (TESS) which will allow us to check the pulsation variability of the stars and to improve the light curve analysis with its high quality photometric data.

To deeply understand the binaries, a combination of the comprehensive spectroscopic and photometric studies are necessary. In this study, we investigated three detached eclipsing binary systems with different  $q$  values. The detailed study of these systems will help us to understand different phenomena in binaries and their evolution. Therefore, similar analyses will improve our knowledge about the binary evolution.

## ACKNOWLEDGMENTS

The authors would like to thank the reviewer for useful comments and suggestions that helped to improve the publication. We thank Çanakkale Onsekiz Mart University Research Foundation (Project No. FBA–2018–2452) for supporting this study. FKA thanks the Polish National Center for Science (NCN) for supporting the study through grant 2015/18/A/ST9/00578. We thank Prof. F. Soyduğan for his helpful suggestions. We are grateful to Dr. E. Niemczura for putting her codes at our disposal. The spectroscopic calculations have been carried out in Wrocław Centre for Networking and Supercomputing (<http://www.wcss.pl>), grant No.214. This paper makes use of data from the first public release of the WASP data (Butters et al. 2010) as provided by the WASP consortium and services at the NASA Exoplanet Archive, which is operated by the California Institute of Technology, under contract with the National Aeronautics and Space Administration under the Exoplanet Exploration Program. This work has made use of data from the European Space Agency (ESA) mission Gaia (<http://www.cosmos.esa.int/gaia>), processed by the Gaia Data Processing and Analysis Consortium (DPAC), <http://www.cosmos.esa.int/web/gaia/dpac/consortium>. Funding for the DPAC has been provided by national institutions, in particular the institutions participating in the Gaia Multilateral Agreement. This research has made use of the SIMBAD data base, operated at CDS, Strasbourg, France.

## REFERENCES

- Andersen J., 1991, *A&ARv*, 3, 91  
 Asplund M., Grevesse N., Sauval A. J., Scott P., 2009, *ARA&A*, 47, 481  
 Avvakumova E. A., Malkov O. Y., Kniazev A. Y., 2013, *AN*, 334, 860  
 Butters O. W., et al., 2010, *A&A*, 520, L10  
 Catanzaro G., Leone F., Dall T. H., 2004, *A&A*, 425, 641  
 Dervişoğlu A., Pavlovski K., Lehmann H., Southworth J., Bewsher D., 2018, *MNRAS*, 481, 5660  
 Eker Z., Bilir S., Soyduğan F., Gökçe E. Y., Soyduğan E., Tüysüz M., Şenyüz T., Demircan O., 2014, *PASA*, 31, e024  
 Eker Z., et al., 2018, *MNRAS*, 479, 5491  
 ESA, 1997, *ESASP*, 1200,  
 Gaia Collaboration, et al., 2018, *A&A*, 616, A1  
 Gray R. O., Corbally C., 2009, *ssc..book*,  
 Ibanoglu C., et al., 2008, *MNRAS*, 384, 331  
 Iglesias-Marzoa R., López-Morales M., Jesús Arévalo Morales M., 2015, *PASP*, 127, 567  
 Ilijic S., Hensberge H., Pavlovski K., Freyhammer L. M., 2004, *ASPC*, 318, 111  
 Kahraman Aliçavuş F., et al., 2016, *MNRAS*, 458, 2307  
 Kahraman Aliçavuş F., Niemczura E., Polińska M., Helminiak K. G., Lampens P., Molenda-Żakowicz J., Ukita N., Kambe E., 2017, *MNRAS*, 470, 4408  
 Kreiner J. M., 2004, *AcA*, 54, 207  
 Kurucz R. L., Avrett E. H., 1981, *SAOSR*, 391, 391  
 Kurucz R., 1993, *KurCD*, 13,  
 Lacy M., Ridgway S. E., Sajina A., Petric A. O., Gates E. L., Urrutia T., Storrie-Lombardi L. J., 2015, *ApJ*, 802, 102  
 Lenz P., Breger M., 2005, *CoAst*, 146, 53  
 Mashonkina L., 2011, *mast.conf*, 314  
 Niemczura E., et al., 2015, *MNRAS*, 450, 2764  
 Paxton B., Bildsten L., Dotter A., Herwig F., Lesaffre P., Timmes F., 2011, *ApJS*, 192, 3  
 Paxton B., et al., 2013, *ApJS*, 208, 4  
 Paxton B., et al., 2015, *ApJS*, 220, 15  
 Pavlovski K., Southworth J., 2009, *MNRAS*, 394, 1519  
 Pavlovski K., Southworth J., Tamajo E., 2018, *MNRAS*, 481, 3129  
 Pollacco D. L., et al., 2006, *PASP*, 118, 1407  
 Ruciński S. M., 1969, *AcA*, 19, 245  
 Schlafly E. F., Finkbeiner D. P., 2011, *ApJ*, 737, 103  
 Simon K. P., Sturm E., 1994, *A&A*, 281, 286  
 Southworth J., Maxted P. F. L., Smalley B., 2004, *MNRAS*, 351, 1277  
 Southworth J., 2013, *A&A*, 557, A119  
 Southworth J., 2015, *ASPC*, 496, 164  
 Soyduğan F., Aliçavuş F., Bilir S., Soyduğan E., Püsküllü Ç., Şenyüz T., 2015, *AJ*, 150, 55  
 Stassun K. G., Hebb L., Lopez-Morales M., Prsa A., 2009, *arXiv*, arXiv:0902.2548  
 Stępień K., Gazeas K., 2012, *AcA*, 62, 153  
 Torres G., Vaz L. P. R., Sandberg Lacy C. H., 2008, *AJ*, 136, 2158  
 Torres G., Andersen J., Giménez A., 2010, *A&ARv*, 18, 67  
 Udry S., Mayor M., Queloz D., 1999, *ASPC*, 185, 367  
 van Hamme W., 1993, *AJ*, 106, 2096  
 von Zeipel H., 1924, *MNRAS*, 84, 665  
 Wilson R. E., Devinney E. J., 1971, *ApJ*, 166, 605  
 Yakut K., Eggleton P. P., 2005, *ApJ*, 629, 1055  
 Zasche P., 2017, *NewA*, 53, 53  
 Zola S., et al., 2004, *AcA*, 54, 299  
 Zola S., Gazeas K., Kreiner J. M., Ogloza W., Siwak M., Koziel-Wierzbowska D., Winiarski M., 2010, *MNRAS*, 408, 464

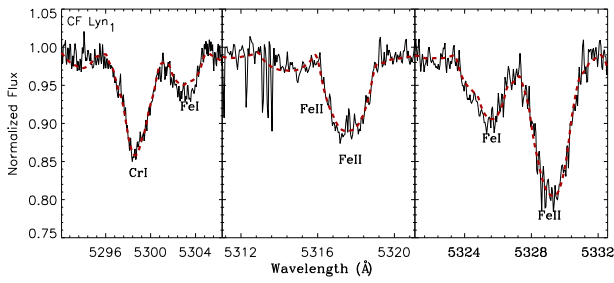
## Appendix

**Table A1.** The  $v_r$  measurements. The subscripts “1” and “2” represent the primary and the secondary component, respectively.

HJD (2450000+)	V2080 Cyg		HJD (2450000+)	V372 And		HJD (2450000+)	CF Lyn	
	$v_{r,1}$	$v_{r,2}$		$v_{r,1}$	$v_{r,2}$		$v_{r,1}$	$v_{r,2}$
1405.3532	-78.4 (4)	85.8 (7)	1930.2801	72.9 (1.4)	-90.0 (2.3)	1930.4271	90.7 (2.3)	-150.8 (5.7)
1407.4062	77.7 (5)	-77.0 (6)	1931.2977	-99.5 (2.7)	133.6 (3.4)	1931.3488	-11.1 (1.3)	
1408.4292	51.0 (4)	-48.7 (5)	1931.4540	-99.0 (3.0)	139.3 (2.2)	2297.5879	84.4 (1.7)	-133.5 (16.4)
1743.4947	76.4 (4)	-75.5 (6)	2299.3294	-76.9 (3.3)	103.3 (3.3)	2299.4022	-75.1 (2.4)	127.2 (11.6)
2042.5990	-26.4 (4)	32.2 (5)	2300.3614	100.9 (1.5)	-126.1 (3.3)	2300.4644	47.6 (1.7)	
2043.5271	60.0 (5)	-56.1 (7)	2302.4076	-49.6 (2.5)	68.7 (2.7)	2302.4815	-62.2 (1.1)	109.3 (10.7)
2490.3749	-75.7 (4)	82.2 (6)	2303.3568	102.3 (2.7)	-128.3 (3.3)	2303.4943	-58.0 (1.9)	101.0 (9.2)
			2490.5689	-66.2 (1.6)	87.4 (2.1)	2303.6085	-86.0 (1.6)	145.0 (13.5)
			2491.5618	103.7 (2.3)	-128.5 (3.1)			

**Table A2.** Abundances of individual elements of the component stars. Number of the analysed spectral parts is given in the brackets.

Elements	V2080 Cyg <sub>1</sub>	V2080 Cyg <sub>2</sub>	V372 And <sub>1</sub>	V372 And <sub>2</sub>	CF Lyn <sub>1</sub>
<sup>6</sup> C	9.31 ± 0.35 (1)	8.80 ± 0.35 (1)	8.72 ± 0.37 (2)	8.29 ± 0.45 (2)	
<sup>11</sup> Na		7.49 ± 0.35 (1)			6.53 ± 0.40 (1)
<sup>12</sup> Mg	7.76 ± 0.35 (3)	7.88 ± 0.31 (2)	7.30 ± 0.37 (2)	7.22 ± 0.45 (2)	7.82 ± 0.38 (2)
<sup>14</sup> Si	7.12 ± 0.32 (5)	7.12 ± 0.30 (4)	7.04 ± 0.35 (7)	7.56 ± 0.46 (1)	6.30 ± 0.38 (2)
<sup>20</sup> Ca	6.33 ± 0.32 (5)	6.03 ± 0.31 (7)	5.93 ± 0.37 (2)	7.40 ± 0.45 (2)	6.29 ± 0.38 (2)
<sup>21</sup> Sc	3.25 ± 0.32 (4)	2.87 ± 0.32 (2)	2.75 ± 0.35 (4)		3.17 ± 0.36 (3)
<sup>22</sup> Ti	4.88 ± 0.32 (17)	5.05 ± 0.31 (17)	5.04 ± 0.30 (25)	5.57 ± 0.40 (8)	5.10 ± 0.30 (24)
<sup>23</sup> V		3.84 ± 0.30 (2)			4.41 ± 0.35 (3)
<sup>24</sup> Cr	5.68 ± 0.26 (14)	5.63 ± 0.30 (23)	6.01 ± 0.32 (24)	6.14 ± 0.38 (11)	5.75 ± 0.30 (17)
<sup>25</sup> Mn	5.20 ± 0.32 (3)	4.93 ± 0.33 (3)	6.28 ± 0.37 (2)	5.51 ± 0.45 (2)	5.52 ± 0.35 (9)
<sup>26</sup> Fe	7.30 ± 0.29 (71)	7.05 ± 0.25 (75)	7.43 ± 0.25 (48)	7.72 ± 0.33 (29)	7.44 ± 0.26 (56)
<sup>27</sup> Co	4.83 ± 0.35 (2)	4.79 ± 0.34 (4)	6.27 ± 0.33 (9)	6.39 ± 0.42 (3)	6.12 ± 0.38 (2)
<sup>28</sup> Ni	6.24 ± 0.32 (15)	6.06 ± 0.31 (15)	6.27 ± 0.33 (9)	6.39 ± 0.42 (3)	6.47 ± 0.30 (22)
<sup>29</sup> Cu			4.52 ± 0.38 (1)		4.16 ± 0.38 (2)
<sup>30</sup> Zn	4.45 ± 0.35 (1)	4.81 ± 0.35 (1)			
<sup>38</sup> Sr					
<sup>39</sup> Y	2.17 ± 0.34 (2)	2.07 ± 0.35 (2)	1.59 ± 0.37 (2)	1.99 ± 0.45 (1)	
<sup>40</sup> Zr					2.84 ± 0.40 (1)
<sup>56</sup> Ba	1.69 ± 0.35 (1)	2.36 ± 0.35 (2)	2.48 ± 0.38 (1)	2.48 ± 0.45 (1)	

**Figure A1.** Comparison of the theoretical (dashed line) and observed spectra (continuous line) of primary component of CF Lyn.